Localization of compressional Alfvén eigenmodes in spherical tori

H. Smith,[a] T. Fülöp, M. Lisak, and D. Anderson
Department of Electromagnetics, Chalmers University of Technology, and Euratom-VR Association, Göteborg, Sweden

(Received 17 December 2002; accepted 18 February 2003)

Edge-localized compressional Alfvén eigenmodes (CAE) may be responsible for the observed emission in the ion cyclotron frequency range in the National Spherical Torus experiments (NSTX) [M. Ono *et al.*, Nucl. Fusion **40**, 557 (2000)]. These modes can be driven unstable by resonant interaction with a small population of energetic ions, having an anisotropic distribution in velocity space. In the present paper, the radial and poloidal structure of these eigenmodes is analyzed, by solving the eigenmode equation using a variational approach. The analysis shows that CAE are radially and poloidally localized near the plasma edge and have eigenfrequencies in the range corresponding to experimentally measured frequencies in NSTX. © *2003 American Institute of Physics.* [DOI: 10.1063/1.1566441]

I. INTRODUCTION

Edge-localized compressional Alfvén eigenmodes (CAE) are currently considered as the main candidate to explain the experimentally observed emission in the ion cyclotron frequency range,[1] in the National Spherical Torus experiments (NSTX).[2] CAE can be destabilized by resonant interaction with a subpopulation of energetic ions [neutral beam injection (NBI) or ion cyclotron resonance heating (ICRH) produced ions], having an anisotropic distribution in velocity space near the outer edge of the plasma. Localized modes are important not only to explain the observed emission, but also because these modes might open a possibility for transferring energy from the fusion products directly to the background ions.

Initial investigations of the localization of the CAE were performed assuming large aspect ratio and frequencies much higher than the ion cyclotron frequency.[3,4] Detailed studies in the limit of circular cross section and infinite aspect ratio,[5,6] have shown that inclusion of the Hall term affects the mode solutions and introduces a dependence on the sign of the poloidal phase velocity. In Ref. 7 the two-dimensional (2D) eigenmode equation, without the Hall term, was analyzed assuming circular cross section. The results indicated that the CAE are localized both radially and poloidally close to the outer midplane edge of the tokamak.

The effects of noncircular cross section, different plasma density profiles and the presence of fast ions were included in Ref. 8, in the limit of infinite aspect ratio, showing that localization of waves of both signs of the poloidal phase velocity is possible provided that the plasma density exceeds a critical magnitude N_{cr} at the outer edge. In Ref. 9 a 2D eigenmode analysis was performed, including the symmetry breaking Hall term, the effect of elliptic cross section, finite aspect ratio and finite parallel wave number. Radially and poloidally localized eigenmodes were found if certain conditions were satisfied. Localization of waves with both signs of the poloidal phase velocity was found to be possible in a finite aspect ratio tokamak with high ellipticity.

The observation of sub-ion cyclotron emission in NSTX at frequencies about half of the ion cyclotron frequency, calls for an extension of the previous eigenmode analysis to be valid also in this frequency range. Ref. 10, analyzed the CAE dispersion in low aspect ratio plasmas, with a number of assumptions, some of which might be of crucial importance for the results.

In the present work we extend the eigenmode analysis to be valid for low mode numbers in spherical tokamak geometry and for frequencies below the ion cyclotron frequency, by using a variational method as in Ref. 10, but with a different Lagrangian functional. In particular, we will keep the Hall term and analyze its effect on the solutions.

The structure of the paper is the following: In Sec. II the 2D eigenmode equation of the CAE is derived. In Sec. III, the eigenmode equation is analyzed with a variational approach. Section IV uses the variational equations to obtain an approximate expression for the eigenmode frequency, and Sec. V presents the numerical solutions to the variational equations. Finally, Sec. VI summarizes our results.

II. THE EIGENMODE EQUATION

We consider compressional Alfvén waves with small parallel wave vector ($k_{\parallel} \ll k_{\perp}$) and with the wave frequency in the range $\omega \sim \omega_{ci} \ll \omega_{ce}$, where ω_{ci} and ω_{ce} are the ion and electron cyclotron frequencies, respectively. The eigenmode equation for the perturbed magnetic field in a cold, inhomogeneous and magnetized plasma with one ion species can be obtained from the Maxwell equations

$$\nabla \times \boldsymbol{B} = \frac{4\pi}{c}\boldsymbol{J}, \tag{1}$$

$$\nabla \times \boldsymbol{E} = \frac{i\omega}{c}\boldsymbol{B}, \tag{2}$$

[a]Electronic mail: elfhs@elmagn.chalmers.se

where it is assumed that the perturbed quantities X depend on time as $\exp(-i\omega t)$, ω is the wave frequency.

Let us introduce the elliptic-toroidal coordinates ρ, ϑ and φ, defined by

$$x=(R_0+\rho\cos\vartheta)\sin\varphi,$$
$$y=(R_0+\rho\cos\vartheta)\cos\varphi, \tag{3}$$
$$z=\kappa\rho\sin\vartheta,$$

where ρ is a radial coordinate, ϑ is the modified poloidal angle, φ is the toroidal angle, R_0 is the major radius of the torus, and κ is the ellipticity of the flux surface defined as the ratio of major to minor radius of the ellipse. The corresponding E_i and B_i are the covariant components of $\boldsymbol{E}$ and $\boldsymbol{B}$. The current in Eq. (1) is $J^i=\sigma^{ij}E_j$, and σ^{ij} is the conductivity tensor being related to the dielectric tensor ϵ^{ij} through $\epsilon^{ij}=\delta^{ij}+i4\pi\sigma^{ij}/\omega$. The conductivity tensor and the metric tensor g^{ij} in elliptic-toroidal coordinates can be found in the Appendix.

We assume vanishing parallel electric field ($E_\varphi+E_\vartheta/q\simeq 0$), where the safety factor is $q=d\Phi/d\Psi$, and Φ and Ψ are the toroidal and poloidal magnetic fluxes, respectively. Furthermore we assume toroidal variation as $X\propto\exp(-in\varphi)$, where n is the toroidal mode number, and we adopt a ballooning representation for the poloidal dependence, cf. Ref. 11

$$X(\rho,\vartheta)=\sum_{j=-\infty}^{\infty}\hat{X}(\rho,\vartheta+2\pi j)e^{inq(\rho)(\vartheta+2\pi j)}, \tag{4}$$

where $q(\rho)$ is the safety factor. We assume that $j=0$ is the dominant component.

We use Eq. (2) to express B_ρ and B_ϑ in terms of E_ρ, E_ϑ and derivatives of E_ϑ and insert this into Eq. (1) to get

$$\frac{\partial B_\varphi}{\partial\rho}=\left(in^2\frac{c}{\omega}\frac{\rho\kappa}{R}g^{11}+\frac{4\pi\sqrt{g}}{c}\sigma^{11}\right)E_\rho+\left(in^2\frac{c}{\omega}\frac{\rho\kappa}{R}b_1+\frac{4\pi\sqrt{g}}{c}\sigma^{12}\right)E_\vartheta, \tag{5}$$

$$\frac{\partial B_\varphi}{\partial\vartheta}=\left(in^2\frac{c}{\omega}\frac{\rho\kappa}{R}g^{21}+\frac{4\pi\sqrt{g}}{c}\sigma^{21}\right)E_\rho+\left(in^2\frac{c}{\omega}\frac{\rho\kappa}{R}b_2+\frac{4\pi\sqrt{g}}{c}\sigma^{22}\right)E_\vartheta, \tag{6}$$

where b_1 and b_2 are

$$b_1=g^{11}\frac{q'}{q^2}-\frac{g^{11}}{nqw_\rho}-\frac{g^{12}}{nqw_\vartheta}, \tag{7}$$

$$b_2=g^{12}\frac{q'}{q^2}-\frac{g^{12}}{nqw_\rho}-\frac{g^{22}}{nqw_\vartheta}, \tag{8}$$

and w_ρ and w_ϑ are the characteristic radial and poloidal length scales of $\hat{E}_\vartheta$, respectively. The two last terms in b_1 and b_2 can be neglected if

$$w_\rho\gg\frac{n}{q}\frac{\rho\kappa}{R^2}\frac{v_A^2(\omega_{ci}^2-\omega^2)}{\omega_{ci}\omega^3} \tag{9}$$

and

$$w_\vartheta\gg\frac{n}{q}\frac{\kappa^2}{R^2}\frac{v_A^2(\omega_{ci}^2-\omega^2)}{\omega_{ci}\omega^3}, \tag{10}$$

which is satisfied in the parameter range of interest.

We now use Eq. (1) together with Eqs. (5) and (6) to express the covariant components of the electric field, E_ρ and E_ϑ, in terms of the toroidal covariant component of the magnetic field B_φ

$$E_\rho=-\frac{1}{c_n}\left(a_4\frac{\partial B_\varphi}{\partial\rho}+a_2\frac{\partial B_\varphi}{\partial\vartheta}\right), \tag{11}$$

$$E_\vartheta=\frac{1}{c_n}\left(a_3\frac{\partial B_\varphi}{\partial\rho}+a_1\frac{\partial B_\varphi}{\partial\vartheta}\right), \tag{12}$$

where the constants a_j are

$$\begin{pmatrix}a_1 & a_2\\ a_3 & a_4\end{pmatrix}=\epsilon_{xx}\frac{\omega}{c}\begin{pmatrix}-R\omega/\omega_{ci}-i\sqrt{g}g^{12}(K_n+1) & -\sqrt{g}g^{12}K_nq'/q^2-i\sqrt{g}g^{22}\\ -i\sqrt{g}g^{11}(K_n+1) & R\omega/\omega_{ci}-\sqrt{g}g^{11}K_nq'/q^2-i\sqrt{g}g^{21}\end{pmatrix} \tag{13}$$

and

$$c_n=a_1a_4-a_2a_3, \tag{14}$$

$$K_n=\frac{n^2v_A^2}{R^2\omega_{ci}^2}\frac{\omega^2-\omega_{ci}^2}{\omega^2}, \tag{15}$$

$g=\det g_{ij}=r^2R^2\kappa^2$, and $R=R_0+\rho\cos\vartheta$. The dielectric tensor elements in Cartesian coordinates with the z axis parallel to the magnetic field can be simplified to

$$\epsilon_{xx}=\epsilon_{yy}=\frac{\omega_{pi}^2}{\omega_{ci}^2-\omega^2},\quad \epsilon_{xy}=-\epsilon_{yx}=i\frac{\omega}{\omega_{ci}}\epsilon_{xx}, \tag{16}$$

where ω_{pi} is the ion plasma frequency.

Taking the third component of Eq. (2)

$$\frac{\partial E_\vartheta}{\partial\rho}-\frac{\partial E_\rho}{\partial\vartheta}=i\frac{\omega}{c}\frac{\sqrt{g}}{R^2}B_\varphi, \tag{17}$$

and using Eqs. (11) and (12), we arrive at the following eigenmode equation for B_φ:

$$\frac{\partial}{\partial\rho}\left\{\frac{1}{c_n}\left(a_3\frac{\partial B_\varphi}{\partial\rho}+a_1\frac{\partial B_\varphi}{\partial\vartheta}\right)\right\}+\frac{\partial}{\partial\vartheta}\left\{\frac{1}{c_n}\left(a_4\frac{\partial B_\varphi}{\partial\rho}+a_2\frac{\partial B_\varphi}{\partial\vartheta}\right)\right\}=\frac{i\omega}{c}\frac{\sqrt{g}}{R^2}B_\varphi, \tag{18}$$

where $B_\varphi \simeq RB_\parallel - B_\vartheta/q$ is the toroidal component of the perturbed magnetic field. We now assume that q'/q^2 is not very large and make the approximation $K_n \ll 1$, which is acceptable if n is low. Using the ballooning representation (4) for B_φ the eigenmode equation (18) can now be rewritten as

$$\frac{ic}{\omega}\left\{\frac{\partial}{\partial\rho}\left[\frac{1}{c_n}\left(a_3\frac{\partial\hat{B}}{\partial\rho}+a_1\frac{\partial\hat{B}}{\partial\vartheta}\right)\right]+\frac{\partial}{\partial\vartheta}\left[\frac{1}{c_n}\left(a_4\frac{\partial\hat{B}}{\partial\rho}+a_2\frac{\partial\hat{B}}{\partial\vartheta}\right)\right]+\frac{in\vartheta q'}{c_n}\left[2a_3\frac{\partial\hat{B}}{\partial\rho}+(a_1+a_4)\frac{\partial\hat{B}}{\partial\vartheta}\right]+\frac{inq}{c_n}\left[(a_1+a_4)\frac{\partial\hat{B}}{\partial\rho}+2a_2\frac{\partial\hat{B}}{\partial\vartheta}\right]\right\}+V(\rho,\vartheta)\hat{B}=0. \tag{19}$$

The potential $V(\rho,\vartheta)=H+iG$ becomes

$$H(\rho,\vartheta)=\frac{\sqrt{g}}{R^2}-n^2(q^2g^{22}+2qq'\vartheta g^{12}+(q')^2\vartheta^2g^{11})\times\frac{v_A^2\sqrt{g}}{\omega^2R^2}+\frac{n}{\omega}\left(q\frac{\partial}{\partial\rho}-\vartheta q'\frac{\partial}{\partial\vartheta}\right)\left(\frac{v_A^2}{R\omega_{ci}}\right) \tag{20}$$

and

$$G(\rho,\vartheta)=\frac{n}{\omega^2}\left[\left(g''\vartheta+q'\vartheta\frac{\partial}{\partial\rho}\right)\left(\frac{v_A^2\sqrt{g}g^{11}}{R^2}\right)+\left(q\frac{\partial}{\partial\rho}+2nq'+q'\vartheta\frac{\partial}{\partial\vartheta}\right)\left(\frac{v_A^2\sqrt{g}g^{12}}{R^2}\right)+q\frac{\partial}{\partial\vartheta}\left(\frac{v_A^2\sqrt{g}g^{22}}{R^2}\right)\right]. \tag{21}$$

In Eq. (19), toroidal effects have been included in v_A and ω_{ci} through the poloidal dependence of the equilibrium magnetic field, which is assumed to fall off as $1/R$. The term in H involving derivatives with respect to ρ and ϑ originates from the Hall term, which has been included in the infinite aspect ratio limit in Refs. 5, 6, and 8. Note that this term breaks the poloidal symmetry even when the inverse aspect ratio is negligibly small. This term is large at the edge, where the plasma density profile is steep and its derivative is large.

III. VARIATIONAL ANALYSIS

For real $\hat{B}$, the Lagrangian corresponding to Eq. (19) is given by

$$L=\xi(\rho,\vartheta)\left[g^{11}\left(\frac{\partial\hat{B}}{\partial\rho}\right)^2+g^{22}\left(\frac{\partial\hat{B}}{\partial\vartheta}\right)^2+2g^{12}\left(\frac{\partial\hat{B}}{\partial\rho}\right)\left(\frac{\partial\hat{B}}{\partial\vartheta}\right)\right]+H(\rho,\vartheta)\hat{B}^2, \tag{22}$$

where

$$\xi=-\sqrt{g}\epsilon_{xx}/c_n=-\frac{\rho\kappa v_A^2}{R\omega^2}. \tag{23}$$

Let $\mathcal{L}=\int d\rho d\vartheta L(\rho_0,\Delta,\vartheta_0,\eta)$ and assume an ansatz function of the form

$$\hat{B}(\rho,\vartheta)=B_0h_s\left(\frac{\rho-\rho_0}{\Delta}\right)h_p\left(\frac{\vartheta-\vartheta_0}{\eta}\right), \tag{24}$$

where $h_s(x)=H_s(x)e^{-x^2/2}$ and $H_s(x)$ is the Hermite polynomial of degree s. The variational principle $\delta\mathcal{L}=0$ now determines the localization radius ρ_0, the radial localization width Δ, the localization angle ϑ_0, the poloidal localization width η and the eigenmode frequency ω. The equation $\partial\mathcal{L}/\partial\vartheta_0=0$ for the variation with respect to ϑ_0 has the solution $\vartheta_0=0$, and to find the rest of the parameters we expand $H(\rho,\vartheta,\omega)$ around ρ_0 and ϑ_0 and assume that $\xi(\rho,\vartheta,\omega)$ is slowly varying around ρ_0 and ϑ_0. The variations with respect to ρ_0, Δ, η and B_0^2 now give the following set of four equations:

$$4\left.\frac{\partial H}{\partial\rho}\right|_{\rho_0,\vartheta_0}+f_s\Delta^2\left.\frac{\partial^3H}{\partial\rho^3}\right|_{\rho_0,\vartheta_0}+f_p\eta^2\left.\frac{\partial^3H}{\partial\vartheta^2\partial\rho}\right|_{\rho_0,\vartheta_0}=\frac{2\xi(\rho_0,\vartheta_0,\omega)}{\eta^2\rho_0^3}[2\kappa^{-2}f_p+\eta^2(1-\kappa^{-2})\times(10p^2-2p+3)], \tag{25}$$

$$\left.\frac{\partial^2H}{\partial\rho^2}\right|_{\rho_0,\vartheta_0}\frac{\Delta^4}{\xi(\rho_0,\vartheta_0,\omega)}=2-\eta^2f_p(1-\kappa^{-2}), \tag{26}$$

$$\left.\frac{\partial^2H}{\partial\vartheta^2}\right|_{\rho_0,\vartheta_0}\frac{\Delta^2\eta^4\rho_0^2}{\xi(\rho_0,\vartheta_0,\omega)}=2\Delta^2\kappa^{-2}+\eta^4\rho_0^2f_s(1-\kappa^{-2}), \tag{27}$$

$$-4H(\rho_0,\vartheta_0,\omega)\eta^2\Delta^2\rho_0^2\xi(\rho_0,\vartheta_0,\omega)^{-1}=\eta^2\rho_0^2f_s(4-\eta^2f_p(1-\kappa^{-2}))+\Delta^2(4\kappa^{-2}f_p+\eta^2(1-\kappa^{-2})(10p^2-2p+3)), \tag{28}$$

which determine the four parameters ω, ρ_0, η, and Δ. Here we have used the notation $f_N=2N+1$.

The main difference between Ref. 10 and our work is the different Lagrangian functionals, caused by the choice of polarization and the neglect of the Hall term in Ref. 10. The different Lagrangians will naturally lead to considerably different results, both the resulting eigenmode frequency and the radial and poloidal localization parameters will be different.

IV. EIGENMODE SOLUTIONS

We will here perform a simplified analysis using Eqs. (26)–(28) neglecting the Hall term and the q'-terms, to obtain an approximate expression for the eigenfrequency. We assume that n, s and p are low. H then becomes

$$H=\frac{\sqrt{g}}{R^2}\left(1-n^2q^2g^{22}\frac{v_A^2}{\omega^2}\right). \tag{29}$$

By evaluating the second derivatives of H and rewriting Eqs. (26) and (27) neglecting the small second terms on the right hand sides we get

$$-\frac{\rho_0\omega^2}{Rv_A^2}+\frac{n^2q^2}{\kappa^2\rho_0^2}\frac{1}{R}(2(\kappa^2R-R_0)+\rho_0)=\frac{2}{\kappa^2\eta^4\rho_0^2} \tag{30}$$

and

$$\frac{\omega^2}{v_A^2}\frac{R_0}{\rho_0R^2}+\frac{n^2q^2}{\kappa^2\rho_0^2}\frac{R_0^2+5R_0\rho_0+10\rho_0^2}{\rho_0^2R^2}=\frac{1}{\Delta^4}, \tag{31}$$

where $R=R_0+\rho_0$. Equation (28) becomes

$$\left(\frac{\omega}{v_A}\right)^2=\left(\frac{nq}{\kappa\rho_0}\right)^2+\frac{f_s}{\Delta^2}+\frac{f_p}{\kappa^2\eta^2\rho_0^2}+\frac{1-\kappa^{-2}}{4\rho_0^2}(10p^2-2p+3). \tag{32}$$

For low n, s and p the first term on the right hand side of Eq. (32) is dominant. Using that term to approximate ω^2/v_A^2 in (30) and (31) gives us expressions for η and Δ, which inserted in (32) result in the eigenfrequency

$$\omega_{|n|,s,p}\simeq\frac{v_A}{\rho_0}\sqrt{\frac{n^2q^2}{\kappa^2}+k_p+\frac{|n|q}{\kappa}\alpha_{sp}}, \tag{33}$$

where k_p and α_{sp} are

$$k_p=(1-\kappa^{-2})(10p^2-2p+3)/4,$$

$$\alpha_{sp}=f_s(\rho_0/R)\sqrt{1+(3+R_0/\rho_0)^2}+f_p\sqrt{1-R_0/(\kappa^2R)}.$$

In expression (33), in contrast to the case of a conventional tokamak with circular cross section, the second and third terms are of the same order as the first one, unless n is large.

Inserting (33) into Eqs. (30) and (31) we obtain better approximations for the localization widths:

$$\frac{1}{\Delta^4}=\frac{1}{\rho_0^2R^2}\left[\frac{n^2q^2}{\kappa^2}\left(\left(\frac{R_0}{\rho_0}+3\right)^2+1\right)+\left(k_p+\frac{|n|q}{\kappa}\alpha_{sp}\right)\frac{R_0}{\rho_0}\right], \tag{34}$$

$$\frac{1}{\eta^4}=n^2q^2\left(\kappa^2-\frac{R_0}{R}\right)-\frac{\kappa^2}{2}\frac{\rho_0}{R}\left(k_p+\frac{|n|q}{\kappa}\alpha_{sp}\right). \tag{35}$$

For moderate s or p, we see that Eq. (35) yields an imaginary value of η^2, and thus we have no solution to our eigenmode equation. This does not necessarily mean that such a set of parameters s and p is unphysical, though. There could be eigenmodes that are simply spread out poloidally. For high s and p, Eqs. (34) and (35) are not valid because of our assumptions.

We can now proceed to calculate the frequency splitting due to discrete n, s, and p. The experimentally observed peaks of NSTX shot #103701 appear in two bands, spanning 0.7–1.2 MHz and 1.5–2.2 MHz. The peaks are separated by a spacing of about 120 kHz. Parameters relevant to the NSTX experiment are: Major radius $R_0=85$ cm, minor radius $a=65$ cm, ellipticity $\kappa=1.6$, ion cyclotron frequency at the edge $f_{ci}=2.3$ MHz and Alfvén velocity at the edge $v_{A,\mathrm{edge}}=10^8$ cm/s.

The frequency splitting because of the toroidal mode number n is according to Eq. (33) determined by

$$\omega_{|n|+1,s,p}^2-\omega_{|n|,s,p}^2=\frac{v_A^2q^2}{\kappa^2\rho_0^2}\left((2|n|+1)+\frac{\kappa}{q}\alpha_{sp}\right). \tag{36}$$

Assuming $\rho_0=45$ cm and $q=1.2$ at the localization point we obtain a frequency splitting for $n=-5$ of about 270 kHz.

The splitting due to the radial quantum numbers s becomes

$$\omega_{|n|,1,0}^2-\omega_{|n|,0,0}^2=2v_A^2|n|q/(\kappa\rho_0R)\sqrt{1+(3+R_0/\rho_0)^2}, \tag{37}$$

giving $\Delta f_s\simeq 420$ kHz for $n=-5$, and the splitting due to the poloidal quantum number is

$$\omega_{|n|,0,1}^2-\omega_{|n|,0,0}^2=2\frac{v_A^2}{\rho_0^2}(1-\kappa^{-2}+|n|q/\kappa\sqrt{1-R_0/(\kappa^2R)}), \tag{38}$$

which gives $\Delta f_p\simeq 260$ kHz for $n=-5$.

Note, that in deriving the simplified expression for the eigenfrequency we have assumed low poloidal quantum numbers, p, (since the higher ones lead to eigenmode frequencies which are higher than the ion cyclotron frequency), while Ref. 10 assumes large p (denoted by m in Ref. 10).

V. NUMERICAL RESULTS

For the numerical solutions of the variational equations we have modeled the plasma density profile by $n(\rho)\propto(1-(\rho/a)^2)^\sigma$, with $\sigma=0.5$ or $\sigma=1$. The magnetic field is approximately $B(R)=B_0R_0/R$ in the low to medium beta NSTX plasmas,[10] where B_0 is the magnetic field at the plasma center. The q-profile is here modeled by $q=q_0(1-\beta(\rho/a)^2)^{-\alpha}$, where $\beta=1-(q_0/q_a)^{1/\alpha}$.

The system of variational equations (25)–(28) was solved numerically, and localized solutions were found with frequencies less than the ion cyclotron frequency at the outboard edge of the plasma. Localization radii and eigenmode frequencies for numerical solutions using the parameter values $\sigma=0.5$, $q_0=1$, $q_a=5$, and $\alpha=1/8$ are shown in Fig. 1.

Note that no solution was found for the case $n=-4$, $s=1$, $p=0$. The numerics show that this is due to the q'-terms in H. If they had been neglected, we would have got a solution for this setup of mode numbers too.

Figure 2 shows the values of the localization widths Δ and η from the same calculations. We see that the eigenmodes are generally more localized for higher $|n|$. For higher s and p the poloidal localization width becomes larger and the radial localization width gets smaller. Also note that, although Eq. (35) is a simplified expression for η, it behaves qualitatively in the same way as the numerical solutions. η is for instance more sensitive to s than it is to p.

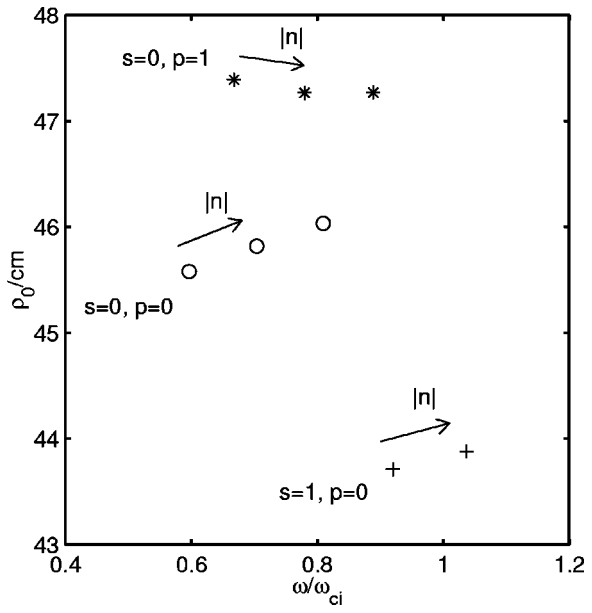

FIG. 1. Solutions of the variational equations with $\sigma=0.5$ for the three cases $\{s=0,\ p=0\}$ (a Gaussian magnetic field ansatz), $\{s=1,\ p=0\}$ and $\{s=0,\ p=1\}$. The arrows for $|n|$ start at the solution where $n=-4$ and point towards higher $|n|$, except for $\{s=1,\ p=0\}$, where it starts at $n=-5$. For $\{s=1,\ p=0,\ n=-4\}$ no solution was found.

The coupling between j and $j\pm1$ terms in the ballooning representation (4) is small because of the small values of the poloidal localization width η. This is analyzed in more detail in Ref. 10.

The frequency splitting due to n is roughly in agreement with the simplified analysis in Sec. IV. The n-splitting is about 240 kHz, while the s-splitting is 500 kHz and the p-splitting is 180 kHz for $n=-5$. The discrepancy between the simplified analysis and the numerics is mainly a result of neglecting the Hall term in Sec. IV.

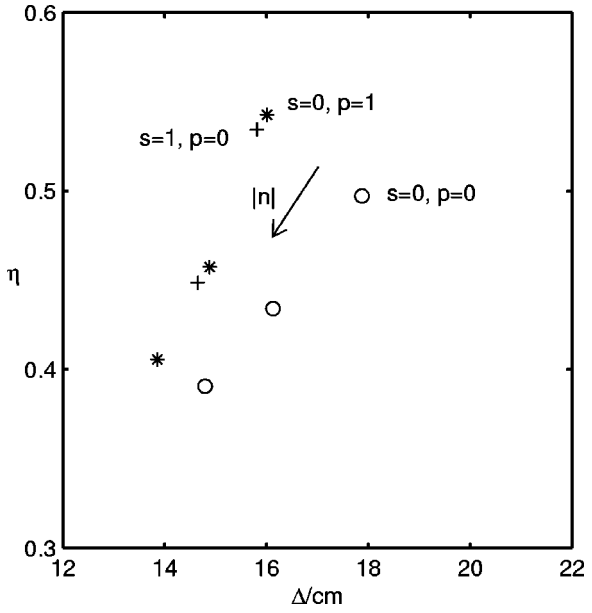

FIG. 2. The Δ and η values of the same solutions as in Fig. 1. $n=-4$ for the rightmost solutions in the cases $\{s=0,\ p=0\}$ and $\{s=0,\ p=1\}$, and for $\{s=1,\ p=0\}$ the rightmost solution is $n=-5$. $|n|$ increases towards the left.

As can be seen in Fig. 1, a combination of the lowest order eigenmode with higher order Hermite polynomial modes may explain that the NSTX experiment has denser peaked spectrum than our calculated n splitting.

Other numerical solutions of the variational equations show that, though the localization radius is rather insensitive to the mode numbers, it depends on the density parameter σ. For $\sigma=0.5$, the eigenmode structure is radially wider and localized closer to the edge, compared to $\sigma=1$. The q-profile also affects the numerical solutions. The effect of increasing q_a and α is that the localization radius decreases and the eigenmode frequency increases.

Because of the Hall term, the solutions are not symmetrical with respect to the sign of the toroidal mode number. For $n>0$, no solutions were found numerically. The existence of localized solutions is affected by the sign of the Hall term, which depends on the radial derivative of the magnetic field and the density profile.

VI. CONCLUSION

The present analysis shows that the poloidally and radially edge-localized CAE have eigenfrequencies in the range corresponding to experimentally measured frequencies in NSTX. The solutions for higher toroidal mode numbers are better localized. A combination of the lowest mode and higher order Hermite polynomial eigenmodes may explain the frequency splitting between the peaks in the experimentally observed spectrum. The Hall term breaks the symmetry with respect to the sign of n, and excludes solutions for positive n.

For relating with the NSTX experimental data, apart from wave localization, also the resonance condition needs to be satisfied and a positive growth rate has to be found. These issues are out of the scope of this paper.

ACKNOWLEDGMENT

This work was supported by the European Community under an association contract between Euratom and Sweden.

APPENDIX: THE METRIC AND CONDUCTIVITY TENSORS

In a tokamak plasma with elliptical cross section we use elliptic-toroidal coordinates, with the contravariant metric tensor, cf. Ref. 12

$$
\begin{aligned}
&g^{11}=\kappa^{-2}\sin^2\ \vartheta+\cos^2\ \vartheta,\\
&g^{22}=(\sin^2\ \vartheta+\kappa^{-2}\cos^2\ \vartheta)/\rho^2,\\
&g^{12}=g^{21}=(\kappa^{-2}-1)\sin\ \vartheta\ \cos\ \vartheta/\rho,\\
&g^{33}=R^{-2},\\
&g^{13}=g^{31}=g^{23}=g^{32}=0,\\
&\sqrt{g}=\kappa\rho R,
\end{aligned}
\tag{A1}
$$

where κ is the ellipticity of the flux surface defined as the ratio of major to minor radius of the ellipse and g is the determinant of the covariant metric tensor.

In Cartesian coordinates with $\hat{z}\|\mathbf{B}_0$ the conductivity tensor has the elements $\sigma_{xx}=\sigma_{yy}=\sigma_{zz}$ and $\sigma_{yx}=-\sigma_{xy}$ and the rest of the elements are zero. Transforming this to the elliptic-toroidal coordinate system we can write the contravariant conductivity tensor σ^{ij} as

$$\sigma^{ij}=\begin{pmatrix} \sigma_{xx}g^{11} & \sigma_{xx}g^{12}+\sigma_{xy}qd_1d_2 & -\sigma_{xy}g^{11}d_2/d_1 \\ \sigma_{xx}g^{21}-\sigma_{xy}qd_1d_2 & \sigma_{xx}g^{22} & -\sigma_{xy}g^{11}d_2/d_1 \\ \sigma_{xy}g^{11}d_2/d_1 & \sigma_{xy}g^{11}d_2/d_1 & \sigma_{xx}g^{33} \end{pmatrix}, \tag{A2}$$

where $d_1=R/(\rho\kappa)$ and $1/d_2^2=q^2R^2+\rho^2\kappa^2g^{11}$. In our case, assuming that $(Rq/(\rho\kappa))^2\gg 1$, we can use the approximation

$$\sigma^{ij}=\begin{pmatrix} \sigma_{xx}g^{11} & \sigma_{xx}g^{12}+\sigma_{xy}(\rho\kappa)^{-1} & 0 \\ \sigma_{xx}g^{12}-\sigma_{xy}(\rho\kappa)^{-1} & \sigma_{xx}g^{22} & 0 \\ 0 & 0 & \sigma_{xx}g^{33} \end{pmatrix}. \tag{A3}$$

[1] E. D. Fredrickson, N. Gorelenkov, C. Z. Cheng *et al.*, Phys. Rev. Lett. **87**, 145001 (2001).
[2] M. Ono, S. M. Kaye, Y.-K. M. Peng *et al.*, Nucl. Fusion **40**, 557 (2000).
[3] B. Coppi, S. Cowley, R. Kulsrud, P. Detragiache, and F. Pegoraro, Phys. Fluids **29**, 4060 (1986).
[4] B. Coppi, Phys. Lett. A **172**, 439 (1993).
[5] B. Coppi, G. Penn, and C. Riconda, Ann. Phys. (N.Y.) **261**, 117 (1997).
[6] G. Penn, C. Riconda, and F. Rubini, Phys. Plasmas **5**, 2513 (1998).
[7] N. N. Gorelenkov and C. Z. Cheng, Nucl. Fusion **35**, 1743 (1995).
[8] YA. I. Kolesnichenko, T. Fülöp, M. Lisak, and D. Anderson, Nucl. Fusion **38**, 1871 (1998).
[9] T. Fülöp, YA. I. Kolesnichenko, M. Lisak, and D. Anderson, Phys. Plasmas **7**, 1479 (2000).
[10] N. N. Gorelenkov, C. Z. Cheng, and E. Fredrickson, Phys. Plasmas **9**, 3483 (2002).
[11] R. D. Hazeltine and J. D. Meiss, *Plasma Confinement* (Addison-Wesley, Redwood City, 1992), p. 203.
[12] YA. I. Kolesnichenko, V. V. Parail, and G. V. Pereverzev, *Reviews of Plasma Physics* (Consultants Bureau, New York, 1992), Vol. 17, p. 1.